Numerical simulation of the hydrodynamic damping of a vibrating hydrofoil

IOP Conf. Series: Earth and Environmental Science **240** (2019) 062002 doi:10.1088/1755-1315/240/6/062002

Numerical simulation of the hydrodynamic damping of a vibrating hydrofoil

E O Tengs [1,2], C W Bergan [1], K-R Jakobsen [2] and P T Storli [1]

[1] Waterpower Laboratory, Norwegian University of Science and Technology, Alfred Getz Vei 4, 7491 Trondheim, Norway

[2] EDR & Medeso AS, Leif Tronstads Plass 4, 1337 Sandvika, Norway

E-mail: erik.tengs@edrmedeso.com

Abstract. The periodic loads from Rotor-Stator interaction is believed to be the main fatigue contributor in High Head Francis turbines. The calculation of the structural response, and thus fatigue, is heavily reliant on the proper hydrodynamic damping characteristics of the water - structure system. The relationship between the water velocity and the hydrodynamic damping is also of great interest. To investigate this, the hydrodynamic damping characteristics of a submerged hydrofoil is simulated in ANSYS CFX. A one-way coupling is implemented, where the blade is forced to vibrate with the first bending mode at the natural frequency, while the hydrodynamic work is calculated over a vibrational period. The velocity of the flow over the hydrofoil is varied in the range v = 2.5 - 45 m/s. Two distinct damping regimes are observed depending on whether the vortex shedding frequency is below or above the lock-in region. The hydrodynamic damping is approximately constant before, and linearly increasing after this region. Experimental data from the Norwegian University of Science and Technology is available for validation, and shows the same trends. The sensitivity with respect to maximum vibrational amplitude is tested, and shows that the hydrodynamic damping is independent of the amplitude as long as the deflections are small.

1. Introduction

Several high head Francis turbines have had failures in the last decades [1, 2]. The reason is thought to be complex fluid-structure interaction in the runner, a resonance issue originating in the pressure field created from the interaction between the stationary and rotating components, known as Rotor-Stator Interaction (RSI) [3]. When designing a turbine, it is desired that the natural frequencies of the structure is far away from the known RSI frequencies. However, the presence of water, a relatively heavy fluid, severely changes structural response under loading. This complicates the calculations of the structural properties. The added mass effects tend to reduce the natural frequencies of the structure, as well as dampening the amplitude of the excitation [4]. In some rare situations, the different vibration modes may even change order [5]. Many have tried to obtain a rule of thumb with regards to the reduction of the natural frequencies, however this has not been found, and may not even be possible [4, 5, 6]. When solving for the frequency response in a submerged Francis turbine, a coupled acoustic-structural simulation is therefore necessary. A crucial input to such simulations is the hydrodynamic damping. As additional complexity, the water in a turbine is not stationary, in a high head Francis turbine, the relative

velocity between blade and water may reach v > 40 m/s. The effect of the moving water on the damping is therefore of great interest, and has been studied experimentally earlier [7, 8, 9]. The general trend is that the hydrodynamic damping is increasing as the flow velocity increase. A general recommendation as to the slope is however not obtainable. The maximal flow velocity in the abovementioned experiments was v ≈ 20 m/s. As far as numerical approximations, Monette et al. [10] provided a mathematical description of the hydrodynamic damping phenomena, and Liaghat et al. [11] performed a two-way fluid-structure coupled simulation on the same geometry. Similar experiments at the Norwegian University of Science and Technology have lately reached v ≈ 30 m/s over the hydrofoil, and also investigated the effects of the lock in region on the damping [12]. This article will try to replicate these experiments numerically, i.e. obtain the hydrodynamic damping coefficient in a system where water is flowing over a vibrating hydrofoil at different velocities. A one-way coupling of the fluid and structure will be performed to reduce the computational cost. The effects of the lock-in region on the damping will also be investigated.

1.1. Dynamic systems

Second order oscillating systems have the following form;

$$M\ddot{u} + C\dot{u} + Ku = F \tag{1}$$

Where M, C, K is the mass, damping and stiffness matrices respectively, u denotes the structural deflection, and F is the loading. Dot notation denotes a one-time differentiation with respect to time, meaning $\dot{u}$ represents velocity and $\ddot{u}$ represents acceleration. The structural deflection is assumed to be periodic with amplitude $u = u_o$ and frequency ω; $u = u_o sin(\omega t)$. A crucial input to the above equation is the damping. There exist several different types of damping, in the normal damping model there is viscous, frequency-dependent damping, but there is also material, frequency-independent damping [13]. In water, the viscous damping has been found to dominate the material damping [14]. The scope of this paper is therefore limited to obtaining the viscous damping ratio.

2. Methods

2.1. Hydrodynamic damping

In order to obtain the viscous damping ratio, we need to derive an expression for the damping effects of the water surrounding a structure. The damping ratio, ξ, of a second order system described by equation (1) is by definition [13]:

$$\xi = C(2M\omega)^{-1} \tag{2}$$

However, obtaining the mass and the damping coefficients is not as easy as in a classical mass – spring - damper system. We need to develop other parameters which can replace the unknowns in equation (2). In the following we show that the hydrodynamic work extracted from a CFD analysis help us doing this.

Assuming linear behaviour, the structural deformation, u, can be decomposed into a superposition of the different structural modes, Φ_i , where a mode is the oscillating shape of a system vibrating at its natural frequency [13].

$$u = \sum_{i}^{k} \Phi_i q_i \tag{3}$$

Where q_i is a scaling factor. The second order oscillating structural system, equation (1), can be rewritten using the above definition (using only one mode);

$$\Phi^T M \Phi \ddot{q} + \Phi^T C \Phi \dot{q} + \Phi^T K \Phi q = \Phi^T F \tag{4}$$

Let the coefficients still be denoted M, C, K, F for simplicity. The coefficient of $\ddot{q}$ is usually normalized such that $\Phi^T M \Phi = 1$ [15]. The second order system can now be written as;

$$\ddot{q} + C\dot{q} + Kq = F \tag{5}$$

Damping extracts energy from the blade. We are therefore interested in the work, $W = \int F\, dx$, over a period. The scaling factor will be periodic, $q = q_o sin(\omega t)$, as it follows the structural deflection, per equation (3). Integrating the left-hand side of equation (5) shows that only the first order term, $\int C\dot{q}dq$, yields a non-zero result over a vibrational period. The work is therefore as follows;

$$W = \int C\dot{q}dq = \int_0^T C\dot{q}^2 dt = C \int_0^{2\pi/\omega} [q_0 \omega \cos(\omega t)]^2 dt = C\pi\omega q_0^2 \tag{6}$$

Additionally, the hydrodynamic work, the work from the structure to the fluid, can be defined as:

$$W = -\int_0^T \int_A p \cdot \dot{u}_n dA dt \tag{7}$$

Where T is one period, p is the fluid pressure, and $\dot{u}_n$ is the velocity of the surface of the structure in the normal direction. Combining equations (2) and (6) finally leads to the definition of the hydrodynamic damping ratio;

$$\xi = \frac{W}{2\pi M \omega^2 q_0^2} \tag{8}$$

Where W is the hydrodynamic work, equation (7), M = 1 [kgm^2] is the modal mass, ω is the angular velocity [rad/s], and q_0 the scaling factor [-]. The hydrodynamic work is obtained from a CFD simulation, the other parameters are obtained from a modal analysis.

2.1.1. Flutter. Hydrodynamic flutter denotes the possibility of negative damping, an instable vibrational system. If certain requirements are met, the fluid flow could transfer energy to the hydrofoil, rather than absorb energy. The system vibration would in that case be self - magnifying, and violent failure could occur. Starting with equation (7). The work per cycle from the fluid to the blade is as follows follows:

$$W = \int_0^T \int_A p \cdot \dot{u}_n dA dt \tag{9}$$

For simplicity we rewrite $p\int dA = F$ to obtain

$$W = \int_0^T \dot{u}_n F dt \tag{10}$$

Assuming harmonic motion of the blade, $u = u_0 sin(\omega t)$ and thus, blade velocity $\dot{u} = \omega u_0 cos(\omega t)$. Let the force follow a similar harmonic motion, oscillating prior to the displacement with a phase angle $\Delta\phi$, $F = F_0 sin(\omega t + \Delta\phi)$. Solving the above integral for one period:

$$W = \omega u_0 F_0 \int_0^{2\pi/\omega} \cos(\omega t)\sin(\omega t + \Delta\phi)dt = \omega u_0 F_0 \sin(\Delta\phi) \quad (11)$$

We see that the work is purely controlled by the phase difference $\Delta\phi$. A positive phase angle indicates that the structure is absorbing energy, an unstable system. Conversely, a negative phase angle will dampen the vibration. A way of visualizing this is the following; if the blade velocity and force is plotted together (recall the integrand in equation (10)), the areas with equal sign of the two functions will contribute to instability. This is shown in figure 1, where the forcing function lags the vibration by $\Delta\varphi = -0.5$. Both the force and blade velocity are scaled to unity amplitude. As the negative area is largest, there is a net energy loss in the blade, and the vibration is damped. Damping is expected in all the simulation in this article, however a difference in phase angle may provide insight into the damping phenomena.

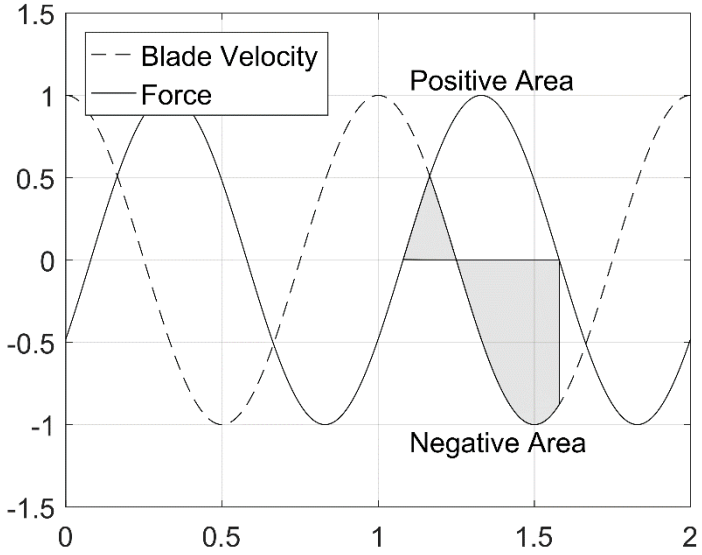

Figure 1. Illustration of phase shift between load and response.

2.2. Experimental setup

The Waterpower Laboratory at The Norwegian University of Science and Technology (NTNU) have performed experiments on both an unsymmetrical hydrofoil (to resemble a Francis turbine blade), and a symmetric hydrofoil. The experimental setup and results from the unsymmetrical test can be found in [12]. The same setup is used for the symmetric hydrofoil tested in this article, some details will be included here.

A symmetric aluminium hydrofoil was excited by electric muscles (Piezoelectric Macrofiber composite actuators from PI Cermaic) to vibrate in a harmonic motion. The hydrofoil was mounted in a stiff 150 mm x 150 mm steel test section, as a part of a longer experimental ⌀ 300 mm pipe system. Several Plexi glass windows were inserted to provide visual access to the blade. Strain gauges and Laser Doppler Vibrometry was used to measure the trailing edge motion. The frequency response was obtained for several different flow velocities and used to calculate the damping characteristics of the system.

Interested readers can find more details in reference [12]. Figure 2 shows a cross-section of the test section, including the placement of the Piezo patches on the aluminum blade. Some global blade dimensions are also included.

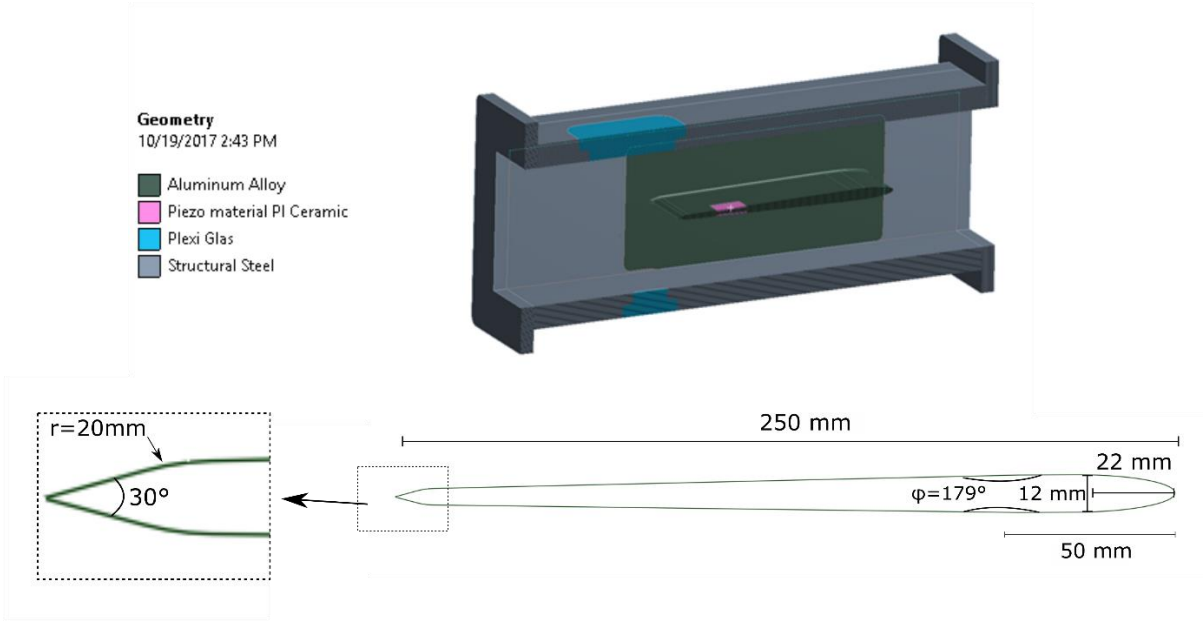

Figure 2. Test section and blade geometry.

2.3. Numerical setup

The work presented in this article tries to replicate the damping characteristics of the symmetric hydrofoil tested at NTNU. Table 1 lists a summary of the most important simulation settings used in this article. The 3 - dimensional numerical domain replicating the experimental rig is shown in figure 3. To ensure that the flow was fully developed before entering the measurement section, the inlet of the domain was extended such that a common entrance length criterion, $> 10D_h$ [16], was satisfied by a large margin. Fully developed flow was verified by testing the inlet turbulence intensity from $0 - 10\%$, with no difference in the levels at the blade. Similarly, the domain was extended downstream to avoid outlet conditions affecting the simulations, and to avoid backflow at the outlet, as the test section is diverging after the blade.

Table 1. Numerical setup.

Software	ANSYS CFX
Turbulence model	$k - \omega$ *SST*
Timestep	7.75e-6 [s] (256 timesteps per period)
Mesh	$5 \cdot 10^6$ elements, all Hexahedral
Deflection amplitude	[2.5, 0.31, 0.05] [mm]
Vibrational frequency	504.37 [Hz]
Boundary conditions	Pressure inlet, mass flow outlet
Flow velocity	2.5 m/s – 45 m/s

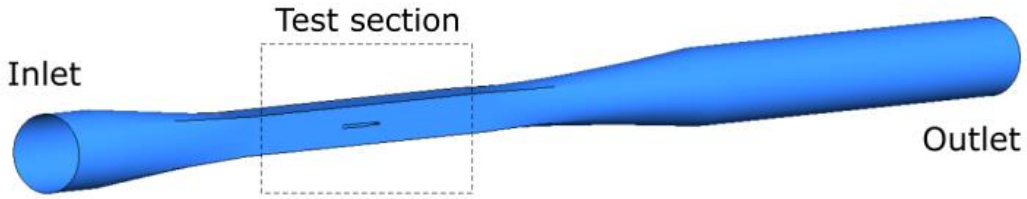

Figure 3. Numerical flow domain.

A one-way coupling was used to obtain the damping. In this case, this means that the structural mode and corresponding natural frequency is calculated in advance. The CFD simulation is then performed with a pre-determined vibrating blade. Constant deflection amplitude is not possible in the experiments, but under the assumption that the damping is primarily dependent on the flow velocity, then it is a reasonable simplification in the numerics. ANSYS CFX was used in the simulations. A specified mass flow was prescribed at the outlet, a zero relative pressure condition at the inlet. The usual no slip condition was prescribed at all walls, and mesh motion forced on the blade surface. A modal analysis was performed in ANSYS Mechanical using the same geometry, with acoustic elements to account for the added mass and stiffness of the water. The first bending mode of the blade corresponds to bending of the trailing edge, and small deflection elsewhere. In a Francis turbine, this is the blade bending mode of interest. This mode shape and corresponding natural frequency was extracted and applied to the blade in CFX. In the simulations, the maximal deflection amplitude was prescribed in advance. The amplitude ranged from 1% to 0.02% of the cord length, i.e 2.5 mm - 0.05 mm as the chord length was 250 mm. A wide range of flow velocities was used, v = [2.5 m/s - 45 m/s] to identify any trends. The hydrodynamic damping was calculated by combining and discretizing equations (7) - (8), meaning that a normalized work was calculated for each timestep and summed over a full vibrational period, see equation (12). Every vibrational period was divided into 256 timesteps. To minimize the effect of the transient start-up on the damping, equation 12 was applied on a periodic solution.

$$\xi = \sum_{k=1}^{256} \frac{-\int_A p \cdot \dot{u}_n dA}{2\pi M \omega^2 q_0^2} \Delta t \tag{12}$$

The mesh consists of hex elements only, created in ANSYS ICEM CFD. The total number of elements was about 5 million, where the damping was found to be independent of element number. Figure 4 shows the mesh in the midplane around the blade, and the same mesh was used in all simulations. The Courant number ($C = u_{local}\Delta t \Delta x^{-1}$) and the y^+ values did therefore change as the free stream velocity was changed, however simulations at v = 30 m/s showed satisfactory values ($C_{rms} = 0.31, y^+_{max} = 2.3$). At the trailing edge, where separation occurs, the y^+ value was well below 1, and verifies the use of the k − ω SST turbulence model [17]. In the mentioned Courant number, u_{local} denotes the local flow velocity, Δt the timestep, and Δx the mesh size. In an explicit solver, this number should be < 1, however this is not necessary in the implicit CFX solver [18].

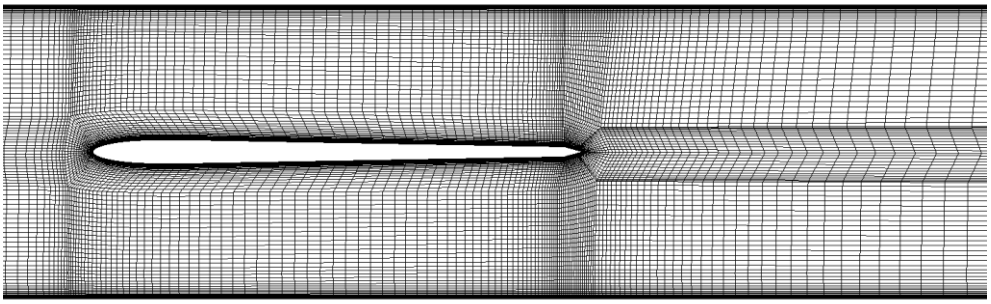

Figure 4. Cross - sectional view of mesh around blade.

3. Results

Figure 5 shows the damping ratio with respect to the flow velocity at three different, fixed amplitudes, $[A_1, A_2, A_3]$ = [2.5, 0.31, 0.05] [mm]. The amplitudes are far apart, A_1/A_2 = 8 and A_2/A_3 = 6.2, however an almost identical behaviour is seen in the simulations using A_2 and A_3. This may indicate that there exists a range of deflections where the hydrodynamic damping factor is independent of the deflection amplitude.

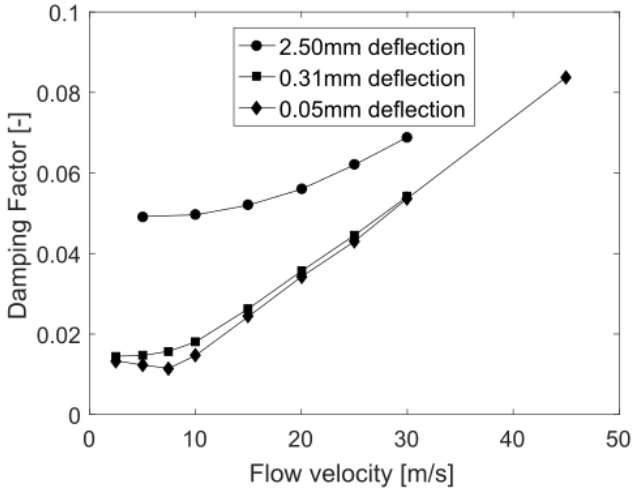

Figure 5. Effect of pre – determined deflection amplitude.

The dependency on the flow velocity however, is not constant or even linear in the whole range. There seems to exist two regions of linear behavior, with different slope. This is supported by experimental results, shown in figure 6. The experimental results are plotted along with an error bar of two standard deviations, and for flow velocities above v = 10 m/s, there is a great match between the experiments and simulations. The large uncertainty at v = 28 m/s in the experiments is due to the onset of cavitation at higher flow velocities. In the experiments, the threshold of v ≈ 6 m/s, marked the lock-in region. Lock-in is the phenomena when the shedding frequency in the flow locks with the natural frequency of the structure over a range of flow velocities, instead of linearly increasing as is reported by i.e. Brekke [19]. A narrow band included in figure 6 for visualization of this region.

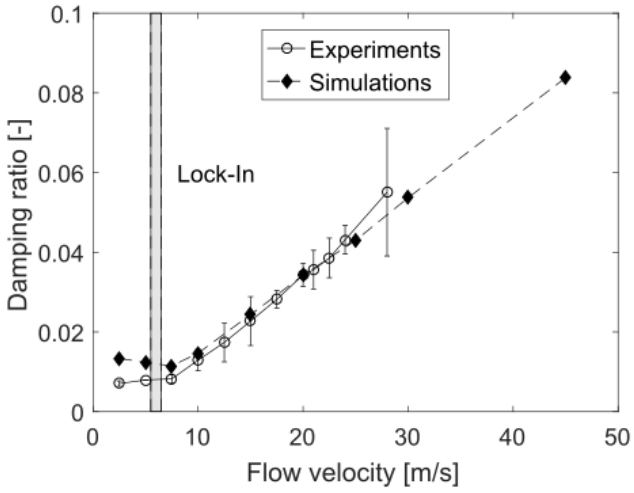

Figure 6. Numerical and experimental damping characteristics.

4. Discussion

Figure 5 indicates that there exists an amplitude range where the damping is independent of the deflection. Moreover, if this range includes the value 0.31 mm, which compared to the blade size is probably unrealistically high, then it can be assumed that the damping is deflection - independent in the whole normal operation range of the turbine. The damping is therefore only a function of the flow velocity, a massive simplification of the system. Similar experiences are seen in the gas turbine industry, however at larger deflections [20]. This result is also supporting the initial assumption of doing a one-way coupled fluid - structure simulation. The second interesting finding is the different damping regions found in figure 6. It is clear that the damping characteristics before and after the lock-in region is different. It should be noted that the simulated and experimental data may not be compared directly, as the deflection amplitude is fixed in the simulations. This is not possible in the experiments. If, however, the assumption of amplitude-independent damping is true, then a comparison could be performed without introducing much error. The phase difference between forcing and vibration, as reviewed in section 2.1.1, is extracted to investigate the damping behaviour more thoroughly by equation (9). Figure 7 (a) shows the phase difference as a function of the flow velocity. The phase difference is obtained by scaling the force on the blade (lift) to unity amplitude and comparing it with the forced vibration (sinusoidal function). The phase is then the spatial difference between the intersection with the x-axis, see small figure in figure 7 (a) or section 2.1.1.

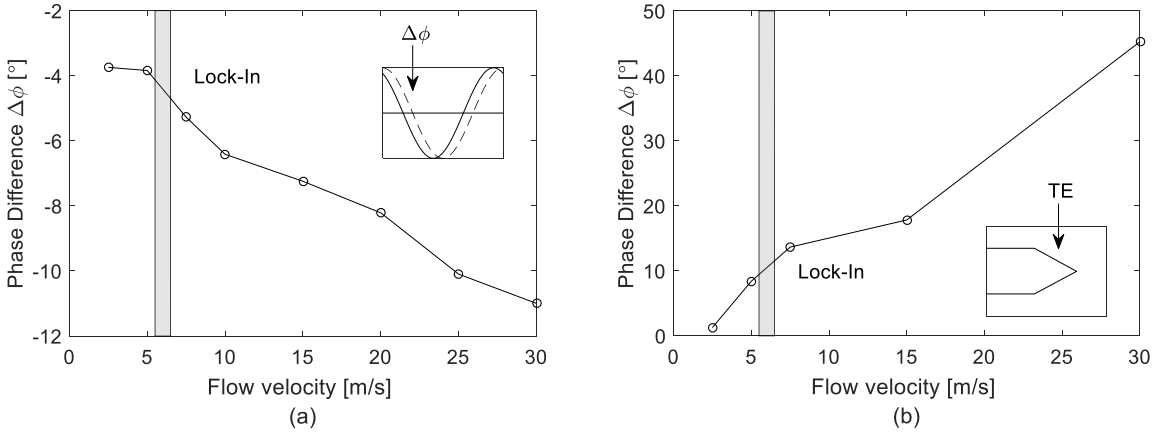

Figure 7. (a) Phase shift, lift whole blade, (b) Phase shift, lift trailing edge only.

We see a change in behaviour before and after the lock-in region here as well, however not as clear as in figure 6. Note that the phase difference is negative for all flow velocities. This indicates that the blade is damped, regardless of flow. An assumption in the derivation of equation (9), is that the velocity of the blade and the pressure on the blade is independent of the location on the hydrofoil. This assumption may not be valid for the mode shape we are studying in this article. To illustrate this, the phase difference using only the lift at the trailing edge (TE in small figure 7 (b)) is extracted and plotted in figure 7 (b). We see that the trailing edge part of the hydrofoil contributes to an unsteady (positive $\Delta\phi$) hydrofoil vibration, although the trend across lock-in is inconclusive.

Looking more closely at the two regions with different damping behaviour. The integrand in the work integral, $(p \cdot \dot{u}_n)$, is composed of two parts. The normal velocity of the blade surface is equal in all simulations, and the pressure is therefore the dimensioning quantity in the integral. The forcing at the trailing edge of the blade is primarily the shedding of vortices. Bergan et al. [12] includes an analytical derivation of the phase shift in the shedding frequency across lock - in, and explains how this may increase the damping at high flow velocities. As was seen in figure 7 (b) the forcing at the trailing edge only was unstable, which actually contradicts this theory. Figure 7 (b) does not indicate that the shedding will dampen the vibration, rather the opposite. However, the assumptions used in deriving equation (9) may be too uncertain to draw any conclusions. Additionally, other factors may dominate the trailing edge shedding, i.e. the development of the pressure field when both the frequency and amplitude is pre-determined in the simulations. A time-consuming two-way coupled simulation may provide further insight. The reason why the damping characteristics changes across the lock-in region is not yet found.

One of the objectives of this numerical and experimental work is to obtain the damping at prototype flow velocities. In a Francis turbine, the relative velocity of the water may easily exceed $v > 40$ m/s. Due to the location of the test rig and the capacity of the pump, the fluid velocity in the experiments was limited to $v \approx 28$ m/s before cavitation occurred. A simulation was therefore run at $v = 45$ m/s, seen in figure 6. We clearly see that the linear trend after the lock-in region is valid even for higher flow velocities. It is therefore reasonable to assume that one can extrapolate the experimental data to higher flow rates.

5. Conclusion

This article shows that a numerical estimation of the hydrodynamic damping of a vibrating hydrofoil is possible. The correspondence with experimental results are very good, especially above the lock-in region. Below this region, the trend is similar, however the absolute values differ somewhat. Two damping regimes are identified; roughly constant before and linearly increasing after the lock-in region. The complete explanation of this phenomena is not known. The hydrodynamic damping is fairly low, $\xi < 0.1$, even for flow velocities realistic to Francis turbines. A one way-coupled simulation was performed, and the vibration amplitude is therefore chosen in advance. This assumption is supported by the result that the damping characteristics are independent of the deflection amplitude, as long as the deflections are small. For larger deflection, a two-way coupling is probably needed.

6. Further Work

The overall goal of the research project is to understand the failure phenomenon in Francis turbines. A key difference from the present geometry and a turbine is the number of blades. In a full turbine, a phase difference in the vibration of two neighboring blades may facilitate negative damping. Therefore, the next iteration of the current study will include several blades to investigate this effect, and increase the similarity to an actual turbine.

Acknowledgments
This work is part of the HiFrancis research project, with financial support from the Research Council of Norway. This support made this work possible.

References

[1] Kobro E 2010 *Measurement of Pressure Pulsations in Francis Turbines* Ph.D. thesis Norwegian University of Science and Technology (http://hdl.handle.net/11250/234140)
[2] Liu X, Luo Y and Wang Z 2016 *Renewable and Sustainable Energy Reviews* **54** 1–14
[3] Seidel U, Hübner B, Löfflad J and Faigle P 2012 *IOP Conf. Series: Earth and Environmental. Science* **15** 052010 ISSN 1755-1315
[4] Dorfler P, Sick M and Coutu A 2012 *Flow-induced pulsation and vibration in hydroelectric machinery* (Springer Science & Business Media)
[5] Liang Q W, Rodrguez C G, Egusquiza E, Escaler X, Farhat M and Avellan F 2007 *Computers & Fluids* **36** 1106–1118 ISSN 0045-7930
[6] Tanaka H 2011 *Int. J. of Fluid Machinery and Systems* **4** 289–306
[7] Coutu A, Seeley C, Monette C, Nennemann B and Marmont H 2012 *IOP Conf. Series: Earth and Environmental. Science* **15** 062060 ISSN 1755-1315
[8] Kaminer A A and Kavitskii B M 1976 *Strength of Materials* **8** 25–27
[9] Roth S, Calmon M, Farhat M, Mnch C, Bjoern H and Avellan F 2009 *Proc. of the 3rd IAHR Int. Meeting of the Workgroup on Cavitation and Dynamic Problems in Hydraulic Machinery and Systems* **1** 253–260
[10] Monette C, Nennemann B, Seeley C, Coutu A and Marmont H 2014 *IOP Conf. Series: Earth and Environmental. Science* **22** 032044 ISSN 1755-1315
[11] Liaghat T, Guibault F, Allenbach L and Nennemann B 2014 *ASME 2014 Int. Mech. Eng. Congress and Exposition* pp V04AT04A073–V04AT04A073
[12] Bergan C W, Solemslie B W, Østby P and Dahlhaug O G 2018 *Int. J. of Fluid Machinery and Systems* **11** 146–153
[13] Craig R R and Kurdila A J 2006 *Fundamentals of structural dynamics* (John Wiley & Sons)
[14] Seeley C 2013 *54th AIAA/ASME/ASCE/AHS/ASC Structures, Structural Dynamics, and Materials Conference* p 1910
[15] ANSYS 2013 *CFX-solver modeling guide* (ANSYS inc)
[16] Yunus A C and Cimbala J M 2006 *Fluid mechanics fundamentals and applications* (McGraw Hill Publication)
[17] Menter F R 1994 *AIAA journal* **32** 1598–1605
[18] Ferziger J H and Peric M 2012 *Computational methods for fluid dynamics* (Springer Science & Business Media)
[19] Brekke H 1994 *Proc. of the 17th IAHR Symp., Beijing, China* pp 15–19
[20] Giersch T, Hnisch P, Beirow B and Khhorn A 2013 *J. of Turbomachinery* **135** 031034